www.czasopisma.pan.pl PAN POLSKA AKADEMIA NAUK www.journals.pan.pl

A R C H I V E S O F M E T A L L U R G Y A N D M A T E R I A L S

Volume 58 2013 Issue 4

DOI: 10.2478/amm-2013-0181

W. PIEKARSKA*, M. KUBIAK*, Z. SATERNUS*

NUMERICAL SIMULATION OF DEFORMATIONS IN T-JOINT WELDED BY THE LASER BEAM

SYMULACJE NUMERYCZNE DEFORMACJI POŁĄCZENIA TEOWEGO SPAWANEGO WIĄZKĄ PROMIENIOWANIA LASEROWEGO

Numerical simulation of deformations in laser welded T-joint is carried out in this study. The analysis is performed using Abaqus FEA engineering software. Additional author's numerical subroutines, written in FORTRAN programming language are used in computer simulations where models of the distribution of movable laser beam heat source, kinetics of phase transformations in solid state as well as thermal and structural strain are implemented. Thermomechanical properties of welded material changing with temperature are taken into account in the analysis.

Presented results of numerical simulations performed for the laser beam welding of two perpendicularly arranged sheets include temperature distribution, kinetics of phase transformations in solid state, thermal and structural strain as well as estimated welding deformations.

Keywords: Laser welding, numerical modelling, welding deformations, T-joint

W pracy przeprowadzono analizę numeryczną deformacji złącza teowego spawanego wiązką laserową. Analizę numeryczną przeprowadzono z wykorzystaniem pakietu oprogramowania inżynierskiego Abaqus FEA. W symulacjach komputerowych wykorzystano dodatkowe, autorskie procedury numeryczne napisane w języku programowania Fortran, gdzie implementowano modele rozkładu mocy ruchomego źródła ciepła wiązki laserowej, kinetyki przemian fazowych w stanie stałym oraz odkształceń termicznych i strukturalnych. W analizie uwzględniono zmienne z temperaturą własności termomechaniczne spawanego materiału.

Przedstawione wyniki symulacji komputerowych wykonanych dla spawania laserowego dwóch prostopadle ułożonych blach obejmują rozkłady temperatury, kinetykę przemian fazowych w stanie stałym, odkształcenia cieplne i strukturalne oraz oszacowane odkształcenia spawalnicze.

1. Introduction

Rapid development of modern production techniques is made in the last few years. The laser beam welding is one of the new concepts of materials joining used in the industry [1, 2]. The development of laser technology has opened new possibilities in many applications, especially in shipbuilding [3, 4]. Due to the advantages of laser beam welding the search began for innovative design solutions progressively replacing traditionally used constructions. Such innovative constructions are "sandwich" type panels [5, 6] consisting of two thin faceplates with a system of stiffeners placed between them, usually arranged in one direction [6]. During laser welding the beam simultaneously penetrates the faceplate and the core joining them together [4, 7]. Joints executed in that way provide high durability, reduced production time and costs. The process proceeds without additional material resulting in the reduction of mass of the entire large-scale welded construction [4, 5]. Moreover, much lower welding deformations occur in laser welded constructions in comparison to conventional welding techniques [8-10].

Important issue in terms of technology is the determination of welding deformations generated at the interface between joined parts and the adjacent area [11-13]. A major problem during laser welding of I-core panels is the deformation of panels surface. Therefore, the development of methods for predicting welding distortion allows for the estimation and evaluation of the quality of welded joints and for the selection of proper process parameters.

In this work the attention is paid to the numerical analysis of thermomechanical phenomena accompanying laser beam but welding of faceplate to core stiffener in "sandwich" panels I-core type. Numerical analysis is based on finite element method performed in Abaqus FEA as three dimensional task. One extracted part form "sandwich" panel is considered in computational model. Geometry of analyzed part consists of perpendicularly arranged plates (T-joint). Temperature dependent thermomechanical properties for S355 steel are assumed in the analysis. Additional subroutines are implemented into Abaqus/Standard solver allowing the determination of movable heat source power distribution, analysis of phase transforma-

* CZĘSTOCHOWA UNIVERSITY OF TECHNOLOGY, INSTITUTE OF MECHANICS AND MACHINE DESIGN FOUNDATIONS, DĄBROWSKIEGO 73, 42-200 CZĘSTOCHOWA, POLAND

tions in solid state and isotropic thermal + structural strain. Welding source power distribution is described by gaussian model. Phase transformations in solid state are analyzed during heating and cooling on the basis of classic kinetics models as well as CHT and CCT diagrams for S355 steel.

2. Finite element 3D model

Three dimensional model was elaborated for laser butt welded two perpendicularly arranged plates made of S355 steel (ferritic - pearlitic structure) with dimensions L =60mm, b =30mm, h =20mm, g =3mm. Scheme of considered system and finite element mesh used in the calculations are shown in Fig. 1. Assumed thermomechanical properties changing with temperature are presented in Table 1.

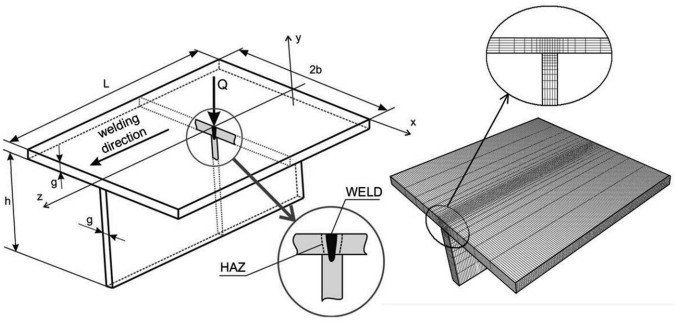

Fig. 1. Scheme of analyzed process with finite element mesh used in calculations

Executed in Abaqus [14] numerical analysis of welded joint deflection is divided into two steps. First step involves analysis of thermal phenomena (thermal analysis) where temperature distribution is obtained as well as parameters necessary to determine the kinetics of phase transformations in solid state. In the second step (mechanical analysis), before estimation of T-joint deflection, the kinetics of phase transformations and isotropic strain are calculated for every finite element in the weld and heat affected zone (HAZ). Both thermal and mechanical analysis uses the same finite element mesh. Dense spatial step of FE mesh is assumed in the weld and heat affected zone to ensure good quality of results. Finite element mesh consists of 26 640 cuboidal elements.

2.1. Thermal analysis

Abaqus/Standard solver is used in thermal analysis. Energy conservation equation and Fourier's law [15] are numerically solved in Lagrange's coordinates, therefore coordinate of heat source $x = v \cdot t$ is defined for every time increment t [s]. The variational formulation of energy conservation equation is expressed as follows:

$$\int_V \rho \dot{U} \delta T \, dV + \int_V \frac{\partial \delta T}{\partial x_\alpha} \cdot \left(\lambda \frac{\partial T}{\partial x_\alpha} \right) dV = \int_V \delta T \, q_V dV + \int_S \delta T \, q_S dS \tag{1}$$

where $\lambda = \lambda(T)$ is a thermal conductivity [W/(m K)], U is a internal energy, q_v is laser beam heat source [W/m^3], q_S is a heat flux toward elements surface [W/m^2], δT is a variational function, ρ is a density [kg/m^3].

Equation (1) is completed by initial condition $t = 0: T = T_o$ and boundary conditions of Dirichlet, Neumann and Newton type with heat loss due to convection, radiation and evaporation as well as welding heat flux towards heated surface taken into considerations. Effective convection-radiation coefficient is assumed in calculations [11, 16-18]. On the surface of laser beam impact, heat dissipation is forced due to the liquid material flow in the fusion zone and blow of shielding gas. Therefore, model proposed by Mundra and DebRoy [17] is used in the analysis. On remaining boundaries of the T-joint Vinokurov model [18] is assumed for constant radiation coefficient (ε =0.5).

Fuzzy solidification front is assumed in the model [19, 20]. Solidus and liquidus temperatures are set to T_S =1477°C (1750K) and T_L =1527°C (1800K), whereas latent heat of fusion H_L =270×10^3 J/kg. Density and specific heat for solid and liquid phase accepted in calculations are given in Table 1.

TABLE 1

Thermomechanical properties used in calculations

Thermal properties				Mechanical properties			
Temperature [°C]	**Conductivity λ [W/m °C]**	**Density ρ [kg/m^3]**	**Specyfic Heat c [J/kg°C]**	**Temperature [°C]**	**Young's Modulus E [GPa]**	**Yield Stress Re [MPa]**	**Poisson Ratio ν**
20	52	7800	650	20	190	320	0.3
200	49	7800	650	400	160	310	0.3
1000	26.5	7800	650	600	130	125	0.3
1477	33.5	7800	650	700	110	60	0.3
1502	34	7300	745	800	40	55	0.3
1527	34	6800	840	900	10	50	0.3
2500	194	6800	840				

In DFLUX subroutine movable heat source power distribution is implemented. Process parameters assumed in calculations are summarized in Table 2. Welding heat source is described by gaussian distribution along radial direction with linear decrease of energy density along material penetration depth [21]

$$q_v(r,z) = \frac{Q}{\pi r_o^2 s} \exp\left[\left(1 - \frac{r^2}{r_o^2}\right)\right]\left(1 - \frac{z}{s}\right) \tag{2}$$

where Q is a laser beam power [W], r_0 is a beam radius [m], $r = \sqrt{x^2 + y^2}$ is actual radius [m], s is penetration depth [m], z is actual penetration [m].

TABLE 2

Process parameters used in computer simulations

Laser beam power	Welding speed	Beam radius	Penetration deep
Q =2 kW	v =0.7 m/min	r_0 =0.7 mm	s =6 mm

2.2. Phase transformations

Numerical estimation of structure composition in laser butt welded T-joint is executed in two additional subroutines HETVAL and UEXPAN used by Abaqus FEA solver. Implementation of HETVAL in thermal analysis allow the determination of maximum temperature (T_{max}) of thermal cycle as well as heating and cooling times (t_h and t_{8-5}) for every finite element in the weld and heat affected zone. Estimated data are further exported to UEXPAN subroutine used in mechanical analysis to calculate kinetics of phase transformations and isotropic strain (thermal and structural strain).

Kinetics of phase transformations in solid state is determined on the basis of classic kinetics of phase transformations models [11, 22, 23] as well as CHT and CCT diagrams for S355 steel [16] interpolated in UEXPAN subroutine. During heating the increase of austenite fraction in the range of austenitization temperatures ($Ac_1(t)$ and $Ac_3(t)$) is defined according to V.I. Machnienko model, expressed as follows:

$$\tilde{\eta}_A(T,t) = 1 - \exp(-k\frac{T_{sA} - T}{T_{sA} - T_{fA}}) \tag{3}$$

where T_{sA} and T_{fA} are start and final temperatures of austenite transformation, factor k is accepted in the range 2.5÷3.

If maximum temperature of thermal cycle is found between $[A_{c1} \div A_{c3}]$ temperatures, then incomplete austenitization occurs. In this case a fraction of austenite formed during heating equals:

$$\eta_A = (T_{\max} - Ac_1(t))/(Ac_3(t) - Ac_1(t)) \tag{4}$$

The analysis of kinetics of diffusive and martensite transformations during cooling is based on V.I. Machnienko model. Transformation of austenite into ferrite, pearlite or bainite is expressed in the following formula:

$$\tilde{\eta}_i(T,t) = \eta^{\%}_{(\cdot)}\tilde{\eta}_A\left(1 - \exp\left(-k\frac{T_s^i - T}{T_s^i - T_f^i}\right)\right) \tag{5}$$

where $\eta^{\%}_{(\cdot)}$ is the final fraction of structural constituent, T_s^i and T_f^i are start and final temperatures of i-th transformation determined for specified cooling time in CCT diagram, $\tilde{\eta}_A$ is a fraction of austenite formed during heating, factor k is within the range 2.5÷3.

Transformation of austenite into martensite is defined as follows [23]:

$$\tilde{\eta}_M(T) = \eta^{\%}_{(\cdot)}\tilde{\eta}_A\left(1 - \exp\left(-k\left(\frac{M_s - T}{M_s - M_f}\right)^m\right)\right),\ T \in [M_s, M_f(v_{8/5})] \tag{6}$$

where M_s and M_f are receptively start and final temperatures of martensite transformation determined for specified cooling time in CCT diagram, while k and m factors are determined experimentally [11].

2.3. Mechanical analysis

Mechanical analysis is performed for laser butt welded T-joint taking into account previously calculated temperature history. Total strain is defined as a sum of elastic, plastic, thermal and structural strain.

$$\varepsilon^{total} = \varepsilon^e + \varepsilon^p + \varepsilon^{TPh} \tag{7}$$

where ε^e is elastic strain, ε^p is plastic strain and ε^{TPh} is isotropic strain generated by temperature field and phase transformations in solid state.

Elastic strain is modelled for isotropic material using Hooke's law with temperature depended Young's modulus and Poisson's ratio presented in Table 1. Plastic flow model is used to determine plastic strain based on Huber-Mises yield criterion and isotropic strengthening [23, 24]. Thermal and structural strain is expressed in increase form:

$$d\varepsilon^{TPh} = \sum_i \alpha_i \eta_i dT - sign(dT) \sum_i \varepsilon_i^{Ph} d\eta_i \tag{8}$$

where $\alpha_i = \alpha_i(T)$ are thermal expansion coefficients of austenite, bainite, ferrite, martensite and pearlite, $\varepsilon_i^{Ph} = \varepsilon_i^{Ph}(T)$ is an isotropic structural strain resulting from the transformation of the base structure into austenite during heating and each phase (ferrite, pearlite, bainite or martensite) arising from austenite during cooling, $d\eta_i$ is a volumetric fractions of phases, sgn (.) is a sign function.

Thermal expansion coefficients and structural strains are determined on the basis of dilatometric analysis [11]. Average values are accepted in computational model. Thermal expansion coefficients and structural strains are set to: $\alpha_1 = 15 \cdot 10^{-6}$ 1/°C – base material, $\alpha_A = 21 \cdot 10^{-6}$ 1/°C, $\varepsilon_A = 3.5 \cdot 10^{-3}$ – austenite, $\alpha_F = 14.7 \cdot 10^{-6}$ 1/°C, $\varepsilon_F = 3.0 \cdot 10^{-3}$ – ferrite, $\alpha_P = 13.7 \cdot 10^{-6}$ 1/°C, $\varepsilon_P = 4.0 \cdot 10^{-3}$ – pearlite, $\alpha_B = 12.5 \cdot 10^{-6}$ 1/°C, $\varepsilon_B = 3.5 \cdot 10^{-3}$ – bainite, $\alpha_M = 12 \cdot 10^{-6}$ 1/°C, $\varepsilon_M = 5.7 \cdot 10^{-3}$ – martensite.

Boundary conditions assumed in mechanical analysis are prescribed for preventing rigid body motion during welding. In marked start position of the laser beam (at the face of the weld) body motion in the x and z directions is prevented. Below this point, at the bottom edge of the I-core, all three degrees of freedom were deprived. Moreover, on the opposite side of the I-core roller support is used allowing free movement of the work piece along z axis. Boundary conditions assumed in mechanical analysis are presented in Fig. 2.

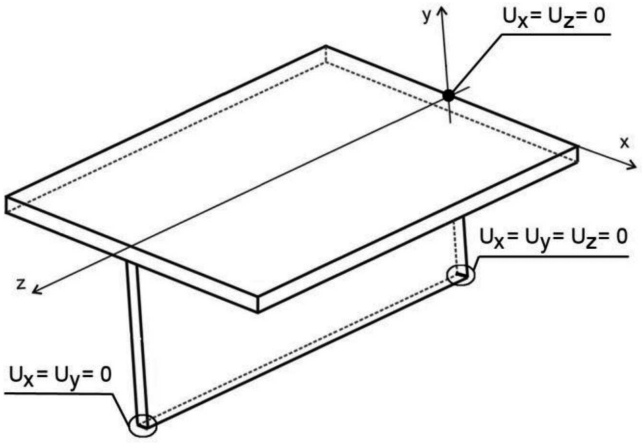

Fig. 2. Boundary conditions assumed in the mechanical analysis

3. Results and discussion

3.1. Results of thermal analysis

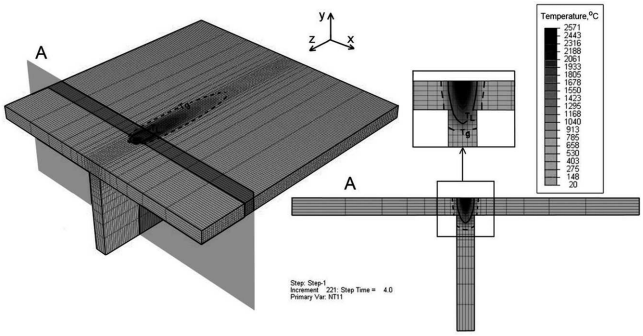

Fig. 3. Numerically estimated temperature field in laser welded T-join

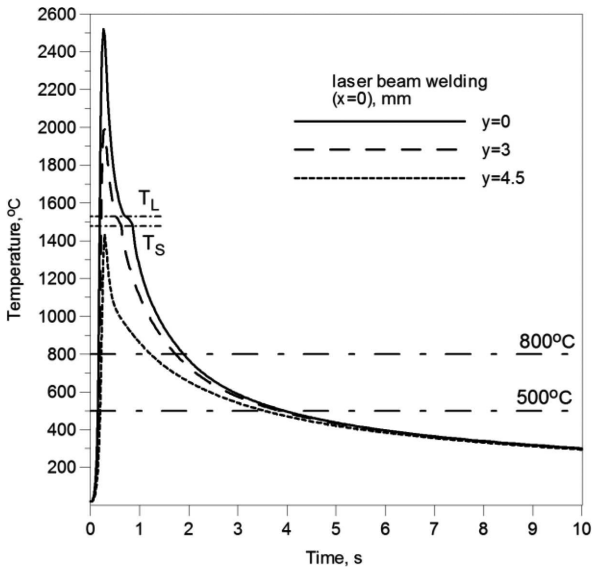

Fig. 4. Temperature distribution in welding line at three various depths of welded joint

Obtained temperature distribution at the top surface and cross section of T-joint butt welded by a laser beam is presented in Fig. 3 where solid line points out the boundary of melted zone (isoline $T_L \approx 1527°C$) and dashed lines indicated the boundary of heat affected zone (isoline Tg ≈ 727°C determined by average austenitization temperature Ac_1). Thermal cycles in welding line at three chosen points in the direction of material penetration are illustrated in Fig. 4 with marked solidus, liquidus temperatures and temperature range [800÷500]°C, within cooling times t_{8-5} are estimated – a basic factor determining phase transformations in solid state.

3.2. Results of mechanical analysis

Predicted isotropic strain (dilatometric curves) with corresponding kinetics of phase transformations in solid state for chosen elements in welding line (x =0) are presented in Fig. 5-7 (at the to surface of the weld, in the middle of the weld and near boundary of heat affected zone).

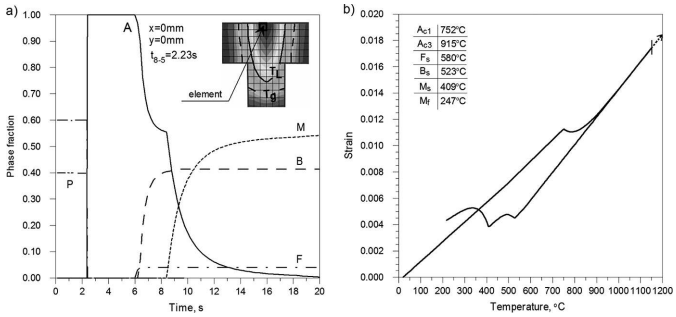

Fig. 5. Calculated a) isotropic strain and b) corresponding kinetics of phase transformations for a chosen thermal cycle placed at the top surface of welded joint. Cooling time t_{8-5} =2.23s

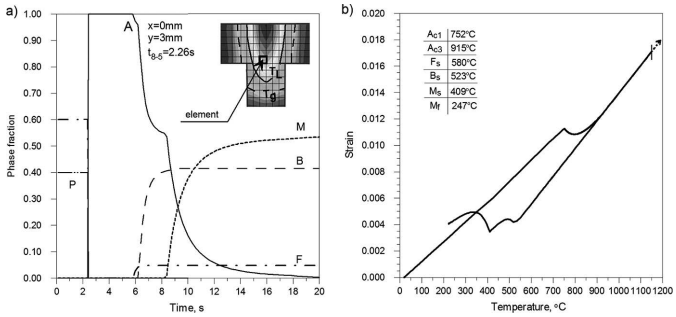

Fig. 6. Calculated a) isotropic strain and b) corresponding kinetics of phase transformations for a chosen thermal cycle placed in the middle of T-joint. Cooling time t_{8-5} =2.26s

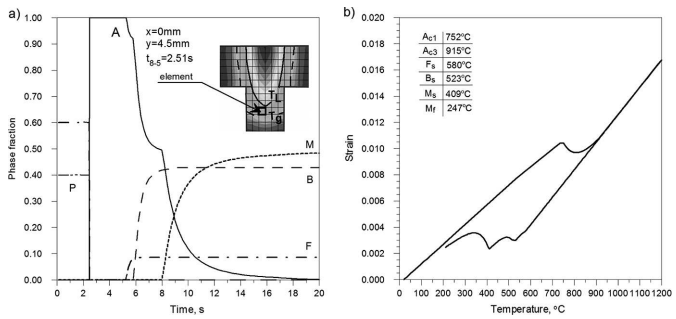

Fig. 7. Calculated a) isotropic strain and b) corresponding kinetics of phase transformations for a chosen thermal cycle placed near the boundary of heat affected zone. Cooling time t_{8-5} =2.51s

Obtained kinetics of phase transformations (Fig. 5-7) shows that structural composition of T-joint consists of bainite, martensite and a minor amount of ferrite. Cooling time

increases with the depth of penetration contributing to the reduction of hardening structures (decreased martensite fraction from 54% to 48%).

Estimated deformation of welded T-joint is illustrated in Fig. 8. Figures 9 and 10 present displacement u_y illustrated as a general deformation field (Fig. 9) and as a deflection of chosen lines along x and z axis (Fig. 10) respectively.

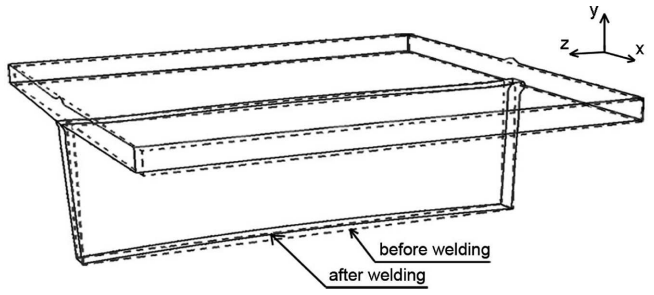

Fig. 8. Estimated deformation in welded T-joint

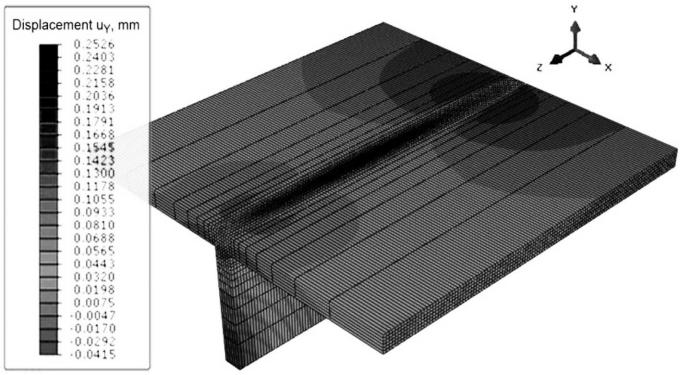

Fig. 9. Distribution of displacement along y-direction

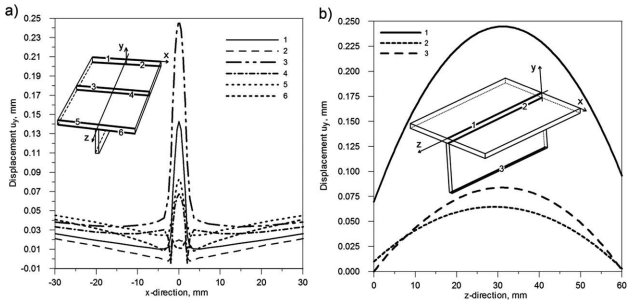

Fig. 10. Estimated deformation of laser welded T-joint. Deflection a) along x axis and b) along z axis

Form calculated deformation of laser welded T-joint (Fig. 10) it can be noticed that due to a small area of thermal impact on the material the deflection in x direction is relatively small and reaches a peak in heat source activity zone. At the top surface of T-joint large vertical deformations occur in the welding line, with the maximum values in the middle of welded faceplate to core stiffener.

4. Conclusions

Obtained results of numerical simulations show that laser beam pass through the faceplate (Fig. 3) joining it with core stiffener (I-core joint) for chosen process parameters. Bainite, ferrite and martensite is formed with a very narrow hardening zone (Fig. 5-7). It can be observed that deflection is symmetrical, relatively small, reaching the peak in a half of the length (L/2) of welded T-joint (Fig. 8-10).

Elaborated numerical models can provide information about the quality of laser welded joint in terms of the use of various process parameters. Performed numerical analysis may be helpful in further developing of "sandwich" panels allowing the selection of proper technological parameters ensuring desired shape of the weld as well as required mechanical properties of the joint.

REFERENCES

[1] W.M. Steen, Laser Material Processing; London; Springer (1991).

[2] A.P. Mackwood, R.C. Cafer, Thermal modelling of laser welding and related processes: a literature review; Opt Laser Technol **37**, 99-115 (2009).

[3] P. Kujala, A. Klanac, Steel Sandwich Panels in Marine Applications; BrodoGradnja **56**, 305-314 (2005).

[4] J. Kozak, All steel sandwich panels – new possibilities introduced by laser welding techniques, Przegląd Spawalnictwa **10**, 53-59 (2007).

[5] T. Urbański, Panele sandwich w wielkogabarytowych konstrukcjach stalowych – charakterystyka problemu łączenia, Postępy Nauki i Techniki **5**, 32-44 (2010).

[6] B. Meteschkow, Sandwich panels in shipbuilding; Polish Maritime Research **S1**, 5-8 (2006).

[7] H. Kolsters, P. Wennhage, Optimisation of laser-welded sandwich panels with multiple design constraints, Mar Struct **22**, 154-171 (2009).

[8] J. Jelovica, J. Romanoff, S. Ehlers, P. Varsta, Influence of weld stiffness on buckling strength of laser-welded web-core sandwich plates, J Constr Steel Res. **77**, 12-18 (2012).

[9] D. Deng, H. Murakawa, FEM prediction of buckling distortion induced by welding in thin plate panel structures; Comp Mater Sci. **43**, 591-607 (2008).

[10] J. Romanoff, P. Varsta, H. Remes, Laser-welded web-core sandwich plates under patch loading, Mar Struct **20**, 25-48 (2007).

[11] W. Piekarska, Numerical analysis of thermomechanical phenomena during laser welding process. The temperature fields, phase transformation and stresses, Wydawnictwo Politechniki Częstochowskiej, Częstochowa (2007).

[12] P. Lacki, K. Adamus, K. Wojsyk, M. Zawadzki, Z. Nitkiewicz, Modeling of heat source based on parameters of electron beam welding process, Arch Metall Mater. **56** (2), 455-462 (2011).

[13] D. Deng, W. Liang, H. Murakawa, Determination of welding deformation in fillet-welded joint by means of numerical simulation and comparison with experimental measurements, J Mater Process Tech. **183**, 219-225 (2007).

[14] SIMULIA, Abaqus analysis user's manual. Version 6.7, Dassault System (2007).

[15] SIMULIA, Abaqus theory manual. Version 6.7, Dassault System (2007).

[16] W. Piekarska, M. Kubiak, Theoretical investigations into heat transfer in laser-welded steel sheets, J Therm Anal Calorim **110**, 159-166 (2012).

[17] K. Mundra, T. DebRoy, Calculation of weld metal composition change in high-power conduction mode carbon dioxide

laser-welded stainless steels, Metall Mater Trans B **24B** (2), 145-155 (1993).

[18] A. De, S.K. Maiti, C.A. Walsh, K.D.H. Bhadesia, Finite element simulation of laser spot welding, Sci Technol Weld Joi **8** (5), 377-384 (2003).

[19] J.M. Dowden, The mathematics of thermal modeling, Taylor & Francis Group, USA (2001).

[20] L. Sowa, A. Bokota, Numerical model of thermal and flow phenomena the process growing of the CC slab, Arch Metall Mater. **56**, 359-366 (2011).

[21] S.A. Tsirkas, P. Papanikos, Th. Kermanidis, Numerical simulation of the laser welding process in butt-joint specimens, J Mater Process Tech. **134**, 59-69 (2003).

[22] S. Serajzadeh, Modelling of temperature history and phase transformations during cooling of steel, J Mater Process Tech. **146**, 311-317 (2004).

[23] A. Bokota, T. Domański, Numerical analysis of thermo-mechanical phenomena of hardening process of elements made of carbon steel C80U, Arch Metall Mater. **52**, 277-288 (2007).

[24] P.M.C.L. Pacheco, L.F.G. de Souza, M.A. Savi, et al., Modeling of quenching process in steel cylinders, Mechanics of Solids in Brazil, Brazilian Society of Mechanical Sciences and Engineering, Brazil, 445-458 (2007).

Received: 20 September 2013.